Fusion Engineering and Design 87 (2012) 1794–1800

Contents lists available at SciVerse ScienceDirect

Fusion Engineering and Design

journal homepage: www.elsevier.com/locate/fusengdes

Characterization of transient particle loads during lithium experiments on the National Spherical Torus Experiment

V. Surla[a,*], M.A. Jaworski[b], V. Soukhanovskii[c], T.K. Gray[d], R. Kaita[b], J. Kallman[b], H. Kugel[b], A. McLean[d], D.N. Ruzic[a], F. Scotti[b]

[a] Center for Plasma-Material Interactions, Department of Nulcear, Plasma and Radiological Engineering, University of Illinois at Urbana Champaign, Urbana, IL 61801, USA
[b] Princeton Plasma Physics Laboratory, Princeton, NJ 08543, USA
[c] Lawrence Livermore National Laboratory, Livermore, CA 94550, USA
[d] Oak Ridge National Laboratory, Oak Ridge, TN 37831, USA

HIGHLIGHTS

- Demonstrated the use of high density Langmuir probe array for characterizing ELMs with a time resolution of 4 μs.
- A methodology was developed to characterize ELMs and ELM statistics are presented.
- An average of 1.5 MW/m^2 and a maximum loading of 7.8 MW/m^2 (with $\gamma = 3$) on the particle flux probe was observed during an ELM in NSTX.
- A correlation was found between particle flux from the probes with D-alpha signal during the ELMs.
- A possible convective nature of ELMs is observed in NSTX discharges with LLD operation.

ARTICLE INFO

Article history:
Available online 17 June 2012

Keywords:
First wall material
Divertor materials
Lithium
Liquid metal
Langmuir probe
Edge localized modes (ELMs)
Particle and power deposition profiles

ABSTRACT

Transient events such as Edge Localized Modes (ELMs) or disruptions can lead to large particle and power loads on the divertor plates of tokamak experiments. These events can cause significant erosion and are detrimental to the lifetime of the plasma facing components. Understanding the impact of ELMs remains a complex problem and a major challenge. In this study, an effort is made to characterize these ELMs and other transients based on their characteristics using a particle flux probe and surface temperature measurements from a dual-band IR camera. Typically, the temporal evolution of an ELM from the particle flux probe is characterized by a steep rise and a gradual decrease of current signal. This burst like structure is seen by the Langmuir probes as a rise in the ion saturation current with a width of a few milliseconds. This study entails gathering statistics of typical ELM-like events for various shots in order to assess the typical loading of ELMs on the Liquid Lithium Divertor (LLD) that was installed in the FY10 run campaign. Later, the power deposition profiles during ELMs are also characterized from IR camera measurements for certain discharges to find that only 15% of the energy flux arrives at the divertor target before the surface temperature reached its maximum value. Finally, a correlation was found between the particle flux from the probes during the ELMs and the neutral particle flux from D_α signal indicating the utility of the particle flux probe as a means to characterize ELMs.

Published by Elsevier B.V.

1. Introduction

Transient events like edge localized modes (ELMs) or disruptions pose a serious problem to the plasma facing component (PFC) material due to intense deposition of power loads on the PFC material. Despite previous experience during lithium experiments showing the suppression of ELMs in NSTX [1,2], liquid lithium divertor (LLD) experiments have been performed when transients were occurring. The power and particle loads associated with these transient events are a significant concern for the NSTX upgrade and next generation devices. The lifetime of the divertor material is associated with the surface temperature exceeding the threshold temperature for evaporation (for a lithium target) or melting (for a tungsten target), leading to significant PFC damage and potential material ejection. Thus, it is important to obtain particle and power deposition profiles on the divertor target during an ELM. In this study, the particle flux profiles are obtained by use of a high density Langmuir probe (HDLP) array. The HDLP array when operated in triple probe configuration gives a time

* Corresponding author. Princeton Plasma Physics Laboratory, Princeton, NJ 08543, USA. Tel.: +1 9704814949.
E-mail address: vijay.surla@gmail.com (V. Surla).

0920-3796/$ – see front matter. Published by Elsevier B.V.
http://dx.doi.org/10.1016/j.fusengdes.2012.05.002

resolution of 4 μs which makes it possible to obtain time resolved ELM characteristics.

In addition, the power deposition profiles are obtained from dual-band IR camera measurements [3]. Initial analysis from the IR measurements was carried out to classify ELMs based on the timescales characterized by the rise time of the surface temperature [4]. The characteristic timescales can give information on the nature of ELMs, either "conductive" or "convective", as classified by Loarte et al. [5]. This analysis is of interest here as it was shown by Loarte et al. [6] that the erosion of the divertor target is lower for convective ELMs and thus represent better operating conditions for the divertor material.

The details of the HDLP array and measurement approach are given in Section 2. The ELM statistics obtained for some of the shots in NSTX along with comparisons of ELM characteristics with IR camera and D_α signals are presented in Section 3 and finally, conclusions are given in Section 4.

2. High density Langmuir probe (HDLP) array

To enhance the edge diagnostic capabilities in NSTX, a HDLP array was installed during the same time as the LLD installation. The HDLP array consists of 99 probes (3 probes/row present in 33 radial rows) that can be operated either as swept probe or as triple Langmuir probes. Each probe electrode is rectangular with a 2 mm radial × 7 mm toroidal cross-section. The HDLP array is located in between the LLD plate segments at a major radius of 62–72 cm and thus covers 1/3 of the LLD radially [7]. Additional details on the HDLP array design and hardware can be found elsewhere [7,8]. In this study, the triple probe configuration is used as it offers, in principle, instantaneous measurements of saturation current and floating potential. The data acquisition captures probe signals at 250 kSamples/s and allows study of fast transient events. However, in order to use the probe for ELM studies, certain modifications have been performed to the circuit in order to increase the particle flux limit reaching the probes.

2.1. Circuit modification

In a traditional triple probe configuration, a constant bias voltage is applied to the probe electrodes as shown in Fig. 1a. Typically, electrode 2 is used to measure floating potential (V_f), electrode 3 is used to measure the saturation current (I_{sat}), and electrode 1 is biased positive and the voltage is measured as V_1. The triple probe configuration allows measurements of the above three parameters from which the electron temperature and number density can be obtained from the equations below [9].

$$T_e = \frac{V_1 - V_f}{\ln 2} \quad (1)$$

$$n = \frac{j_{sat}}{0.6 e C_s} \quad (2)$$

where T_e is the electron temperature, n is the number density, j_{sat} is the ion saturation current density (A/m^2), e is unit electron charge and C_s is the sound speed of ions. However, corrections are often applied to Eq. (1) in order to account for changes in bias voltage and similar effects [8,9]. In order to increase the sensitivity of the probe and improve the signal to noise ratio (SNR) at smaller currents, all the probes are initially designed to collect a maximum current of 2.5 A. However, this places a limit on the particle flux collected during transient phenomenon and so one of the probe configurations was altered to increase the limit on the current signal. For this purpose, the resistance of the sensing resistor is modified such that current signals up to 5 A can be collected with the probe. Further, as the probe draws significant currents during transient events like ELMs or disruptions, the bias voltage applied to the probes can vary. The effect of bias voltage on electron temperature measurements is already reported in [9], and so it is important to understand the response of the bias voltage during transient events. For this purpose, the probe configuration is modified as shown in Fig. 1b. Instead of measuring floating potential from electrode 2, as in conventional triple probe technique, it is modified to measure voltage on electrode 3 such that bias voltage can be measured directly ($U_{bias} = V_1 - V_3$). In a way, floating potential measurements are sacrificed to measure bias voltage. Note that this modified probe can no longer measure floating potential, and thus cannot be used to infer electron temperature from Eq. (1). Because of this, the electron temperature measurements at this location have to be obtained indirectly from the adjacent probes. The effect of the circuit modifications can be seen from Fig. 2. Firstly, in Fig. 2a, the increase in current saturation limit can be seen. The particle flux from an adjacent unmodified probe is also shown for reference. As can be seen in Fig. 2a, the current saturates on the unmodified probe while the reconfigured probe (also referred as particle flux probe in this paper) can measure up to twice the saturation current of 5 A. Secondly, the typical response of the bias voltage as measured from the reconfigured probe is shown in Fig. 2b. As can be seen, the bias voltage does not stay constant and responds in a non-linear way. This behavior is found to vary depending on the duration and amplitude of the current signal as can be seen from different saturation current signal peaks in Fig. 2b. It should be noted that electron temperature

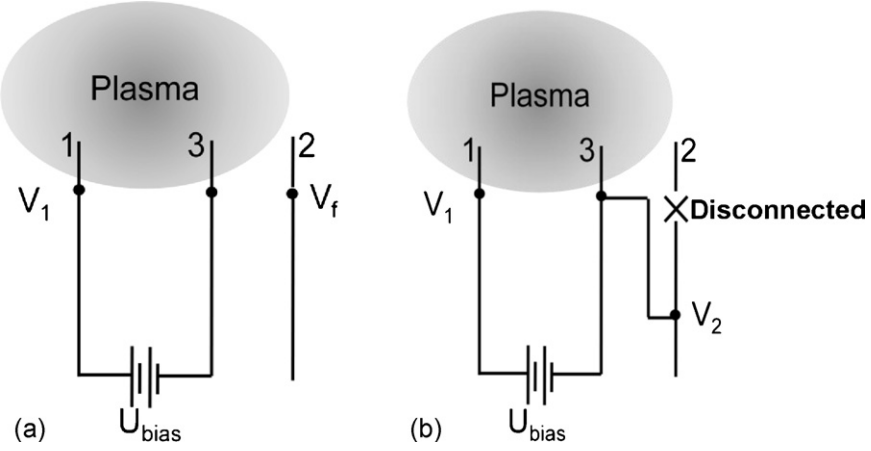

Fig. 1. Schematic of (a) triple probe configuration and (b) particle flux probe configuration. In the particle flux probe configuration, electrode 2 is disconnected from measuring floating potential, and electrode 3 is connected to electrode 2 such that V_3 is measured via V_2. This modification allows measurement of biasing potential, $U_{bias} = V_1 - V_3$.

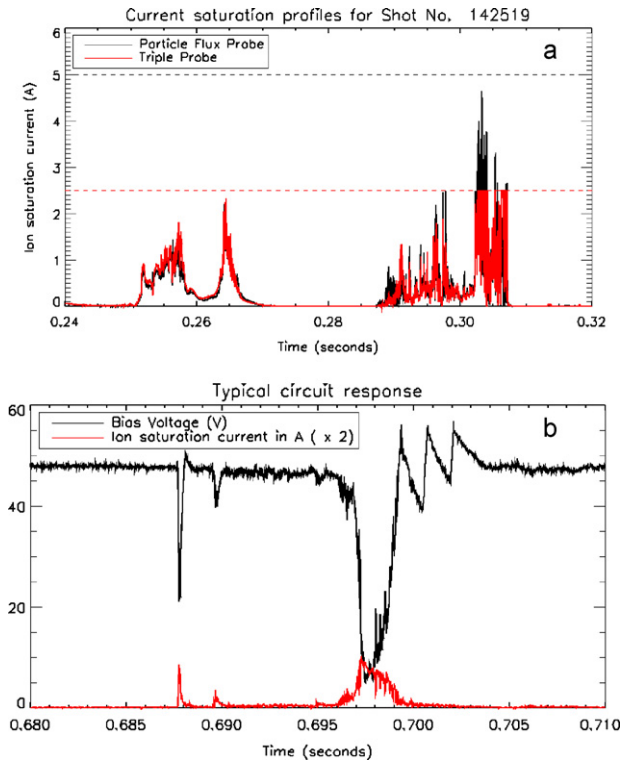

Fig. 2. (a) Ion current as measured from particle flux probe and adjacent unmodified triple probe. Unmodified probe is a very good indicator of temperature at the reconfigured probe. (b) Typical circuit response as measured by the particle flux probe. Instantaneous measurements of bias voltage and ion saturation current can be made from the reconfigured probe. The ion current affects the biasing potential, which varies non-linearly with I_{sat}.

(T_e) measurements cannot be obtained from the reconfigured probe as it no longer measures floating potential, V_f, which is required in Eq. (1) for T_e measurements. However, as can be seen from Fig. 2a, the adjacent unmodified triple probe matches very closely with the current profile of reconfigured probe and thus can act as a very good indicator of the temperature at reconfigured probe. When T_e measurements are required to evaluate the particle power deposition on the target, the unmodified probe can be used to provide a good approximation to what their values might be at the location of the particle flux probe.

2.2. ELM size definitions for the particle flux probe

Typically, the evolution of an ELM is characterized by a steep rise and a gradual decrease of current signal. This burst like structure is seen by Langmuir probes as a rise in the ion saturation current with a typical duration of a few milliseconds as shown in Fig. 3. In this study, three characteristics for ELMs are defined. The time at which the current signal starts to rise is marked as t_0, and time at which it decays back to original signal is marked as time, t_n. The difference between the starting and final times is defined as the duration of the ELM, which is called the characteristic time, τ_{ELM}. The time-averaged area of the current saturation signal for the characteristic time is defined as the characteristic particle flux, Γ_{ELM}. Also, a characteristic power deposited on the probe, q_{TLP}, is defined as the characteristic flux multiplied by the sheath heat transmission coefficient, γ and kT_e. These characteristic quantities are represented by the following equations.

$$\tau_{TLP} = t_n - t_0 \tag{3}$$

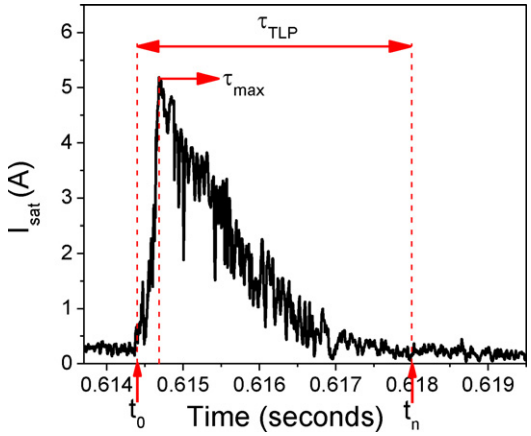

Fig. 3. ELM size definitions for a typical ELM as measured by the particle flux probe.

$$\Gamma_{TLP} = \frac{1}{A_p}\left[\frac{\int (I_{sat}/e)dt}{\tau_{TLP}}\right] \tag{4}$$

$$q_{TLP} = \gamma \times \Gamma_{TLP} \times kT_e = q_{IR} \tag{5}$$

where A_p is the area of the probe surface, I_{sat} is the saturation current, τ_{TLP} is the duration of the ELM, k is the Boltzmann constant, T_e is the electron temperature as measured from the adjacent unmodified probe, q_{IR} is the heat flux measured by the IR camera, and γ is the effective sheath heat transmission coefficient. Fig. 3 shows the ELM size definitions for a typical ELM.

3. Results and discussion

ELMs may be identified by many diagnostics. They appear as clearly defined peaks of short temporal duration on multiple diagnostics such as the D-alpha signal, IR camera temperature signal etc. The time occurrence of the ELM as detected by the particle flux probe agreed well with other diagnostics. For example, the ELM occurrence is shown via particle flux probe signals (I_{sat} and U_{bias}), D_α signal and IR camera heat flux measurements in Fig. 4. It can be seen that there is good overlap of ELM peaks from various diagnostics. The temporal accuracy of the fast IR camera is not good due to randomness inherent in the trigging process for the camera. The result of this random trigger time with respect to the shot clock makes temporal accuracy of the fast IR signal ~±1 ms and so not much significance should be given to the fact that the peak in the heat flux profiles in Fig. 4 between the probes and IR camera do not align perfectly. In addition, it can be seen that the temporal resolution on particle flux probe is (~150 times ×) much higher than the D_α and IR camera signals and so may be an ideal diagnostic to study ELMs.

It should be noted here that the ELM characteristics measured by the particle flux probe are measured only at the major radius of the probe, regardless of where the strike point is located in the shot. Thus, the characteristics are not necessarily indicative of the peak in the ELM radial profile. In the future, the particle flux probes at different radial locations will be used to study spatial characteristics of ELMs. This work only represents initial ELM studies depicting the usefulness of the particle flux probe diagnostic.

3.1. ELM statistics

Having defined the characteristics of ELM size, several shots have been analyzed to obtain statistics on ELMs and determine the effective loading on the LLD during ELMs. Nearly 900 discharges were analyzed and it was found from the particle flux probe that only 375 of those discharges contained ELMs. The

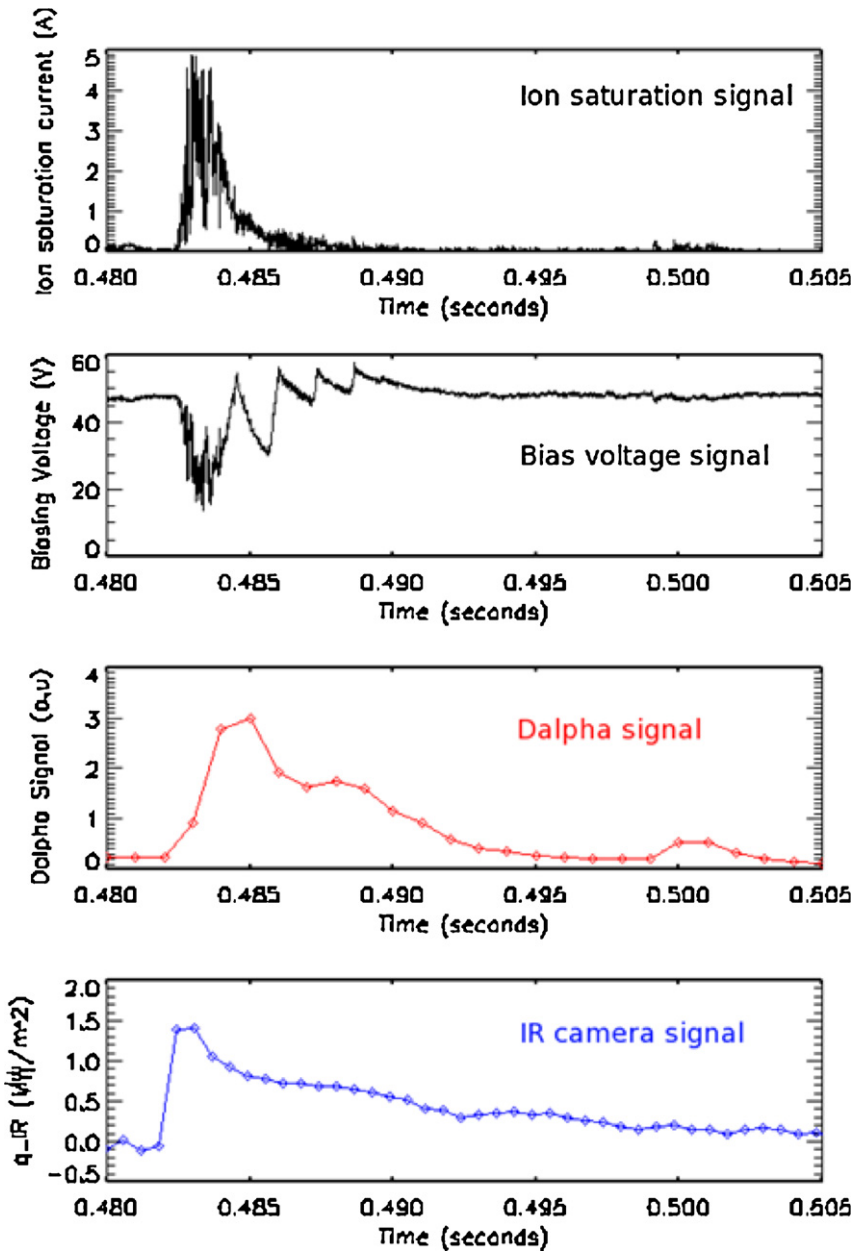

Fig. 4. Time occurrence of a transient event as measured by the I_{sat} signal (a), U_{bias} signal (b), D_α signal (c) and IR heat flux profile (d). The $r - r_{sp}$ value for this data is 12.4 cm.

characteristic quantities defined earlier are obtained for all the 375 discharges to obtain general statistics on the defined quantities in Eqs. (3)–(5). The mean characteristic time of the ELM (τ_{TLP}) was found to be 4 ms ± 1.5 ms, the mean particle flux (Γ_{TLP}) was found to be $3.5 \times 10^{23}/m^2\,s \pm 2 \times 10^{23}/m^2\,s$, and the mean energy deposited (q_{TLP}/γ) was found to be 0.5 MW/m^2. Taking the value for effective sheath heat transmission coefficient (γ) as 3, which is measured recently for NSTX discharges [10], an average particle loading of 1.5 MW/m^2 on the particle flux probe surface is obtained. Note that this entails statistics on all the shots that might not necessarily have the strike point location near the probe. (γ) As it is significantly lower than the standard value of 8 for H plasmas. Kallman et al. obtained this low value for NSTX discharges using classical Langmuir probe interpretation. However, Jaworski et al. [11] recently showed that in NSTX discharges, bimodal plasmas are observed at the LLD and that the classical probe interpretation might not hold. Because of the bimodal distribution, the electron temperatures obtained from classical probe approach could be as high as 2–6 leading to a low value in the sheath heat transmission coefficient [11], While more detailed studies are being planned for future work, it should be noted that the current value for sheath transmission coefficient (γ) is taken as 3 and thus the particle loading values presented in this paper represent the lowest possible values. Fig. 5a shows the histogram plot and cumulative distribution function (c.d.f.) of characteristic flux (Γ_{TLP}) from all the 375 shots that contain ELMs. It can be seen that the distribution is not Gaussian and that more than 75% of the discharges have particle fluxes less than $5 \times 10^{23}/m^2\,s$ as measured by the probe. Similarly, the histogram plot and c.d.f. of characteristic energy deposited on the particle flux probe is shown in Fig. 5b. The distribution is again skewed and more than 70% of the discharges have values less than 0.5 MW/m^2 (with $\gamma = 3$, this is equivalent to a power loading of 1.5 MW/m^2) and has as high value as 2.6 MW/m^2 ($\gamma = 3$ yields 7.8 MW/m^2). This indicates that the maximum loading

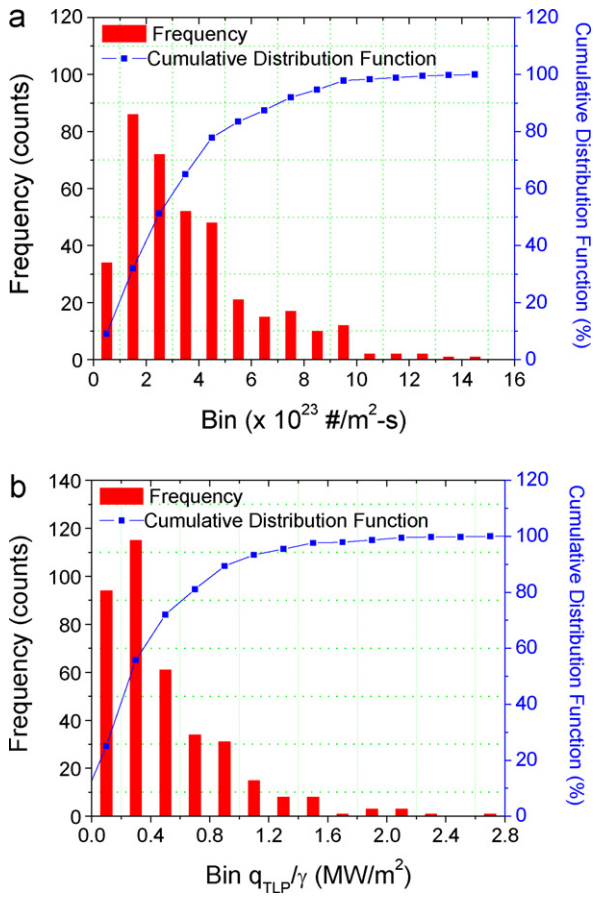

Fig. 5. (a) ELM characteristic flux at the probe, (b) ELM characteristic power deposited at the probe.

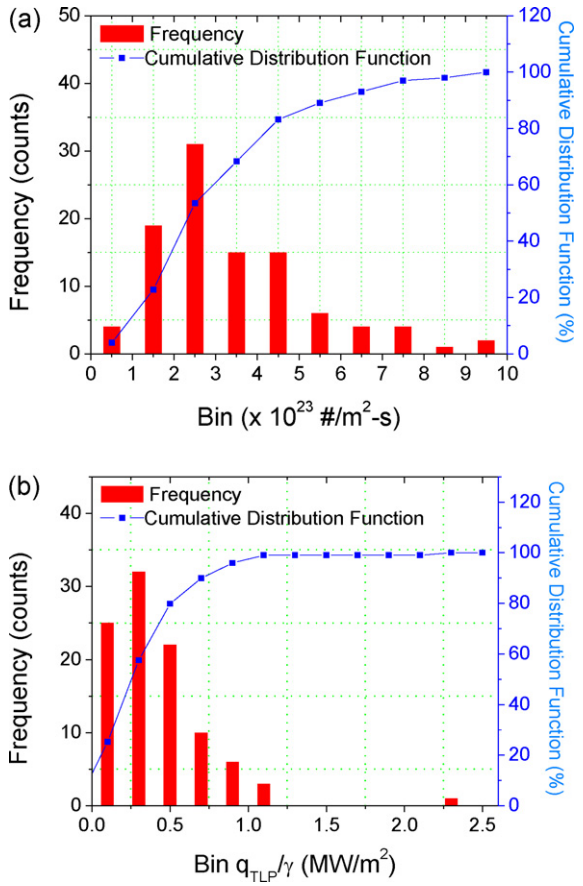

Fig. 6. (a) ELM characteristic flux at the probe, (b) ELM characteristic power deposited at the probe for shots with $|r - r_{sp}| \leq 10$ cm.

experienced by the particle flux probe in all the discharges is as high as 7.8 MW/m^2. It should be noted that the power deposition requires the knowledge of T_e during an ELM. Obtaining T_e during an ELM is challenging as the bias voltage changes non-linearly during an ELM and is part of future investigation. However, in this study, only the average T_e values measured by the adjacent probe before and after the ELM are used for this power deposition calculation. If the analysis is limited to strike point location, r_{sp}, as close as 10 cm to the probe radius, r, only 113 shots have ELMs and if $|r - r_{sp}| \leq 5$ cm, only 46 shots have ELMs. Analyzing only the shots that have $|r - r_{sp}| \leq 10$ cm, the characteristic flux is plotted in Fig. 6a and the characteristic power deposited at the probe is plotted in Fig. 6b. It was found that the mean characteristic flux and energy deposited at the probe for strike point closer to the probe are statistically not different from the mean characteristic values obtained from Fig. 5. This suggests that a new approach is needed to analyze the ELMs based on the total ELM energy and it will be investigated in the future. All the three characteristic parameters defined are prone to measurement errors. There is a systematic measurement error associated with measuring t_0 and t_n of an ELM due to which the characteristic times and flux are prone to error. Also, there is an uncertainty in T_e measurements which leads to large uncertainties in the characteristic power deposited on the particle flux probe. A better way to characterize ELMs, in the future, would be to measure the number of particles (N_{TLP}) and the energy deposited in Joules (E_{TLP}) at the probe using the following equations, wherein there is no dependence of the defined parameters on the characteristic time, τ_{TLP}, and thus the resulting error in the measurement can be avoided. Obtaining T_e during an ELM with good accuracy will be considered in future work.

$$N_{TLP} = \int \left(\frac{I_{sat}}{e}\right) dt \tag{6}$$

$$E_{TLP} = \gamma \times N_{TLP} \times kT_e \tag{7}$$

3.2. ELM characteristics with IR camera

ELMs can also be characterized based on IR camera measurements. The IR camera installed on NSTX provides simultaneous measurements in two wavelength bands to compensate for emissivity changes in the lithium surface and acquires data at a frame rate of 1.6 kHz [3]. The dual-band IR camera is calibrated in situ using view of LLD surface for accurate temperature measurements. The heat conduction code, THEODOR [12], is then used to determine the incident heat flux for the measured temperature change on LLD. These heat flux profiles could also be used to characterize ELMs. As given by Eich et al. [4], the heat flux profile during an ELM can be separated into two phases as can be seen from Fig. 7. In the first phase, the target temperature and thus heat flux rises up to a maximum value and in the second phase, it decays back to the original value. The characteristic timescale (τ_{IR}) is defined as the time it takes for the heat flux signal to increase from 5% above the initial value to the maximum value (100%). The time it takes to reach the peak value for temperature or heat flux is found to be identical and so the τ_{IR} values could be derived using either temperature or heat flux profiles. In this study, the heat flux profiles are used. Also, the fraction of ELM energy deposited before the characteristic time, τ_{IR},

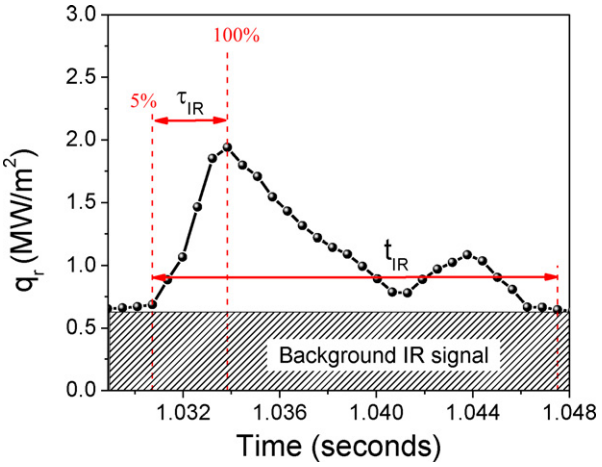

Fig. 7. ELM characteristics for IR camera. Temporal evolution of the power deposition during an ELM event on the divertor target plates at the same radial location, *r*, as the particle flux probe.

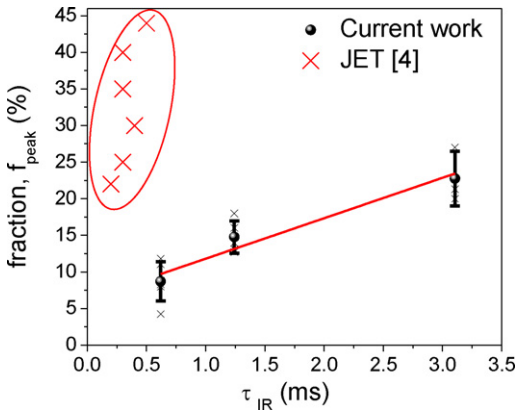

Fig. 8. Correlation between the characteristic time, τ_{IR}, and fraction, f_{peak}. The fraction varies between 5% and 25% in NSTX discharges. Representative values of f_{peak} obtained in JET by Eich et al. [4] are also presented for comparison.

which leads to the maximum temperature rise on the LLD during an ELM can be defined as f_{peak} [4].

$$f_{peak} = \frac{E_{ELM}(t \le \tau_{IR})}{E_{ELM}} \quad (8)$$

$$E_{ELM}(t \le \tau_{IR}) = \int_0^{\tau_{IR}} q_r dt \quad (9)$$

$$E_{ELM} = \int_0^{t_{total,IR}} q_r dt \quad (10)$$

where q_r is the heat flux profile at the same radial location as the particle flux probe, $t_{total,IR}$ is the entire time duration of ELM signal as shown in Fig. 7. E_{ELM} is the energy obtained by taking the time integral of the heat flux profile, q_r, for the entire duration, $t_{total,IR}$. The amount of energy that reaches the divertor target before τ_{IR} is given by $E_{ELM}(t \le \tau_{IR})$. Note that the background area shown in Fig. 6 has to be subtracted from the total integrated area in order to obtain the actual increase in heat flux due to an ELM.

The threshold energy and power fluxes for ELM-induced erosion are determined by τ_{IR} and the amount of energy that reaches the divertor target during this phase, $E_{ELM}(t \le \tau_{IR})$ [6]. If τ_{IR} and $E_{ELM}(t \le \tau_{IR})$ are such that the threshold for divertor material evaporation is not reached, any subsequent heating will not lead to material evaporation, which is the leading erosion mechanism for lithium. A comparison between the particle flux measured by the reconfigured probe and the heat flux profile measured by IR camera provides some qualitative information as can be seen in Fig. 4. It can be clearly seen that the duration of the ELM measured by the particle flux probe is much smaller than the duration of the heat flux profile. For the discharges analyzed, the typical duration, $t_{total,IR}$, of IR heat flux profiles, 20 ms ± 8 ms, is less than the duration of particle flux signal, τ_{TLP}. This suggests that the target continues to get heated even when there is no particle loading on the target which might indicate other sources of heating either due to neutral particle convection and/or local heating due to radiation. Modeling studies will be undertaken in the future to understand the thermal response of the PFC material and isolate the effect of cooling from the characteristic 1/*e* decay times obtained from the model.

ELM characteristics from IR camera diagnostic are analyzed for some discharges in NSTX in order to obtain τ_{IR} and f_{peak} values that are described earlier. From these discharges, the typical times to reach the peak heat flux, i.e., the characteristic IR time, τ_{IR}, on the order of few milliseconds is observed. Further, the dependence of f_{peak} on τ_{IR} is plotted for these discharges as shown in Fig. 8. It can be seen that there is a correlation between the fraction of the energy deposited during the first phase of target heat flux and the characteristic time, τ_{IR}. Further, it can be seen that the f_{peak} values stay below 25% and can be as low as 5% for smaller τ_{IR}. The weighted average of all the f_{peak} values resulted in $f_{peak} = 15 \pm 8\%$ for the discharges investigated in this study. This value is lower compared to the studies in JET [4] where they reported values of $f_{peak} = 32 \pm 8\%$ (also shown in Fig. 8). Loarte et al. [5] classified ELMs as "conductive" or "convective" based on the ELM energy losses associated with the ELM temperature drop and they further showed results in [6] that for convective ELMs, the proportion of the total ELM energy arriving at the divertor target in the interval $[0,\tau_{IR}]$ is as low as 20%. While detailed future experiments are needed to make similar ELM classification studies in NSTX, following the work of Loarte et al., the low values of f_{peak} found for discharges in NSTX suggest that the ELMs are of convective nature. The time scales for the ELM heat flux profiles are much longer such that more than 85% of the ELM energy flux arrives after the divertor temperature has reached its maximum value. These represent favorable operating conditions for the LLD as it is known that erosion is smaller for convective ELMs [6]. The influence of ion transport and formation of a high energy sheath should be investigated in the future studies.

3.3. Comparison with D-alpha measurements

Finally, a comparison is made between particle flux probe and D_α signal measurements. The distribution of neutral particle flux during an ELM can be obtained from D_α diagnostic camera installed on NSTX. This camera acquires D_α profiles at a rate of 5 kHz at a specified radial location. To obtain the time averaged neutral particle flux, the D_α signal is integrated and then divided by the duration of the ELM as measured by the camera at the same radial location as the probe's location. Note that for few shots, the D_α signal saturates as shown in Fig. 9a and for these cases, the integration of the D_α signal does not represent the true neutral flux. The ion particle flux striking the target during an ELM obtained from the reconfigured probe is compared to the neutral particle flux as shown in Fig. 9b. As expected, a correlation can be seen from the ion particle flux and the neutral particle flux indicating the validity of the probe as a suitable diagnostic. Further, it can be seen from Fig. 9b that the ion particle flux exceeding $9 \times 10^{23}/m^2$ s causes saturation on the D_α signal. This clipping behavior of the D_α signal places a

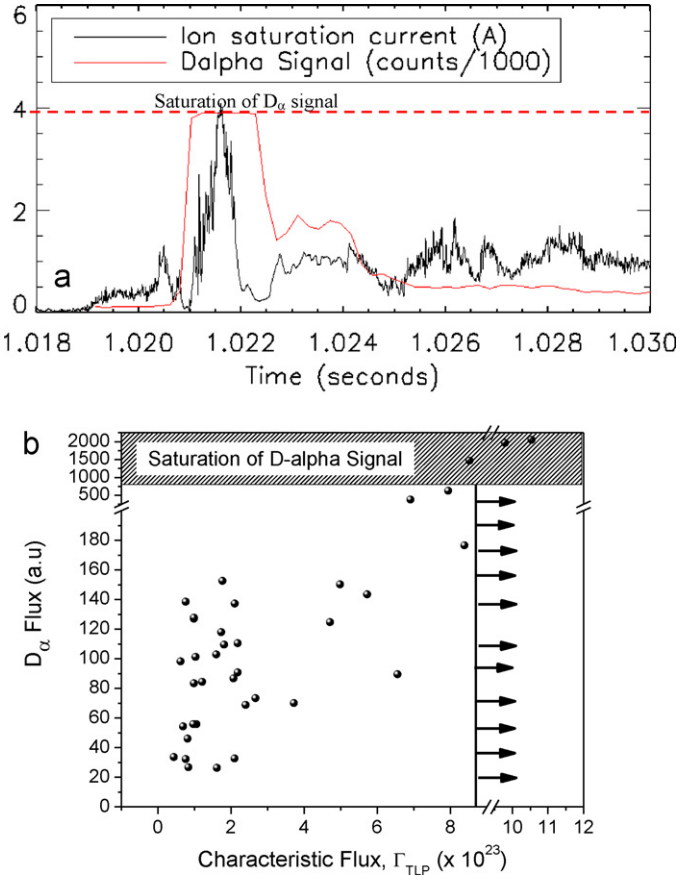

Fig. 9. (a) Saturation of D-alpha signal – D_α signal is divided by 1000 to make it appear on the same scale as I_{sat}. The flat region of the D_α signal denotes the saturation of D_α, (b) Comparison of ion particle flux from particle flux probe with the neutral particle flux from D_α signal.

limitation while the particle flux probe is still able to measure without any saturation Thus, with the current instrumentation for D_α signal on NSTX, the particle flux probe seems to a better diagnostic to characterize ELMs both in terms of time resolution and signal saturation. Future studies will investigate spatial widths of particle flux by reconfiguring the triple probes at various other spatial (radial) locations to study ELMs.

4. Conclusions

This study demonstrates the use of saturation current profiles measured by the Langmuir probes in triple probe configuration as a means to study ELMs with a time resolution of 4 μs. A methodology was developed to characterize ELMs, at a particular radial location of the particle flux probe, and the statistics for some of the NSTX discharges are presented. In the future, using the methodology described here, it is possible to obtain ELM characteristics at different radial locations by making use of the other available electrodes in the HDLP array. In addition, comparisons were made between other diagnostics such as D_α measurements and IR camera measurements. The time resolution on the probe is much higher than the other diagnostics considered here and could be very well used for studies within a single ELM. There is a correlation between the particle flux profiles incident on the probe with the neutral particle flux coming out of the divertor target as measured by D_α signal. Further, the comparison of particle flux measurements with dual-band IR camera measurements suggested some qualitative effects that require future investigation. The duration of the ion current signals are typically shorter than the heat flux profiles and further modeling is required to investigate thermal response of the PFC and understand the sources of heating other than plasma particle loading on the target. Also, it was found that the fraction, f_{peak}, value on an average is found to be 15% for NSTX discharges indicating a possible convective nature of the ELMs with liquid lithium as divertor. These represent favorable operating conditions for the LLD as it is known that erosion is smaller for convective ELMs.

Acknowledgement

This work is supported by DOE contract No. DE-PS02-07ER07-29 and DE-AC02-09CH11466.

References

[1] D.K. Mansfield, H.W. Kugel, R. Maingi, M.G. Bell, R. Bell, R. Kaita, et al., Journal of Nuclear Materials 390–391 (2009) 764.
[2] R. Maingi, T.H. Osborne, B.P. LeBlanc, R.E. Bell, J. Manickam, P.B. Snyder, et al., Physical Review Letters 103 (2009) 075001.
[3] A.G. McLean, J.W. Ahn, R. Maingi, T.K. Gray, A.L. Roquemore, Review of Scientific Instruments 83 (5) (2012).
[4] T. Eich, A. Herrmann, G. Pautasso, P. Andrew, N. Asakura, J.A. Boedo, et al., Journal of Nuclear Materials 337–339 (2005) 669–676.
[5] A. Loarte, G. Saibene, R. Sartori, D. Campbell, M. Becoulet, L. Horton, et al., Plasma Physics and Controlled Nuclear Fusion 45 (2003).
[6] A. Loarte, G. Saibene, R. Sartori, T. Eich, A. Kallenbach, W. Suttrop, et al., Physics of Plasmas 11 (5) (2004).
[7] J.J. Kallman, M.A. Jaworski, R. Kaita, H. Kugel, T.K. Gray, Review of Scientific Instruments 81 (2010) 10E117.
[8] M.A. Jaworski, J. Kallman, R. Kaita, H. Kugel, B. LeBlanc, R. Marsala, et al., Review of Scientific Instruments 81 (2010) 10E130.
[9] M. Laux, Contributions to Plasma Physics 44 (7–8) (2004) 695–699.
[10] J. Kallman, M.A. Jaworski, R. Kaita, H. Kugel, A. McLean, V. Surla, Presented at ISLA conference, Princeton, NJ, 2011.
[11] M. Jaworski, M.G. Bell, T.K. Gray, R. Kaita, J. Kallman, H.W. Kugel, et al., Fusion Engineering and Design (2012), http://dx.doi.org/10.1016/j.fusengdes.2011.07.013.
[12] A. Herrmann, M. Laux, D. Coster, J. Neuhauser, D. Reiter, R. Schneider, Plasma Physics and Controlled Nuclear Fusion 37 (17) (1995).